Capillary force on particles near a drop edge resting on a substrate and a criterion for contact line pinning

Ashok S. Sangani, Changhsin Lu, Kenghsien Su, and James A. Schwarz*
Department of Biomedical and Chemical Engineering, Syracuse University, Syracuse, New York 13244, USA
(Received 6 February 2009; published 9 July 2009)

When a drop of liquid containing particles is allowed to evaporate from a substrate, the flow induced by the liquid evaporating from the drop edge carries the particles to the edge. If these particles prevent the drop edge from receding as the evaporation proceeds, then more particles will be accumulated near the drop edge resulting in the formation of a deposit that resembles coffee rings. We determine the capillary force on the particles near a drop edge and the effect of the particles on the gas-liquid-substrate contact angle to derive a condition that must be satisfied for particles to form the ringlike pattern.

DOI: 10.1103/PhysRevE.80.011603 PACS number(s): 68.08.Bc, 83.80.Hj, 89.90.+n, 47.61.−k

I. INTRODUCTION

Drying of a particle-laden liquid droplet resting on a substrate is both an interesting and an important phenomenon that has attracted several investigations (e.g., Deegan *et al.* [1,2], Popov [3], and Truskett and Stebe [4]). Flow induced by evaporation, together with capillary forces on the particles partially immersed in the liquid, is believed to play an important role in producing interesting patterns of the particles left behind on the substrate when the liquid evaporation is complete. The ring formations when a drop of coffee evaporates from a cup and the salt lines left behind in driveways upon melting of snow and water evaporation are examples of this phenomenon. Recent interest in the phenomenon also arises from potential applications in producing photonic crystals by drying a film of liquid containing small particles (Denkov *et al.* [5,6], Dushkin *et al.* [7], Adachi *et al.* [8], and Gigault *et al.* [9]) and the microfluidic applications relying on the large shear rates generated in thin liquid films from liquid evaporation (Jing *et al.* [10]). Formation of particle rings is undesirable in applications that require uniform deposition of the particles on the substrate and desirable in others, such as jet ink printing, where it aids in producing sharper images.

Deegan *et al.* [1] explained the formation of particle rings as follows. The presence of the particles near the drop edge facilitates the pinning of the contact line at the drop edge separating liquid, gas, and substrate. Since the liquid evaporation rate is the greatest at the edge, the liquid from the bulk of the drop flows outward, toward the edge of the drop, and carries with it the particles resulting in a formation of a particle ring near the drop edge. The mechanism by which the particles facilitate the contact line pinning was not addressed.

In fact, not all particles facilitate the contact line pinning. We have observed in our laboratory (cf. Sec. II) that, while the contact line remains pinned for smaller particles, the contact line and the particles both move toward the center of the drop when particles are not small or if the particle volume fraction is too small. Shmuylovich *et al.* [11] also observed that the contact line does not always remain pinned. These investigators reported that the contact line repeatedly pins and depins as the drop evaporates. The present study aims at understanding why the pinning of the contact line is facilitated in some cases and not in the others. We study in detail the forces acting on particles near the drop edge and the effect of the particles on the contact line angle to derive a criterion for predicting conditions under which the particles will pin the contact line.

In Sec. III, we analyze the problem of determining the capillary force on a particle or a ring of particles protruding from the gas-liquid interface near a drop edge. It is assumed that the drop edge remains circular and pinned. We find that the behavior of the capillary force as a function of the position of the particles for small particles is not significantly different from that for the large particles and that force also does not significantly depend on the number of particles near the drop edge. This suggests that the pinning phenomenon is not directly related to the capillary force acting on the particle. Next, we determine the effect of the presence of the particles on the contact angle at the drop edge. In order that the particles pin the contact line, this angle should be constant or increasing with time as the evaporation proceeds. The effect of the decreasing volume of the liquid due to evaporation is to reduce the contact angle while the opposite is the effect of the protruding particles. If the rate at which the particles arriving at the drop edge increase the contact angle exceeds the rate at which the contact angle is decreased by the evaporation, then the contact line will remain pinned. A criterion is derived for this condition to hold in terms of particle and drop radii and the volume fraction of the particles in Sec. IV. Smaller particle radius and larger volume fractions, both of which lead to greater number of particles near the drop edge, favor the contact line pinning. When the protruding particles are at rest, the viscous drag force, which is proportional to the liquid velocity, is balanced by the capillary force. Since the smaller particles must get much closer to the drop edge before they can protrude from the drop, they also experience larger fluid velocity than the larger particles and this further facilitates the pinning by the smaller particles. The criterion is shown to be in agreement with the limited experimental data obtained in our laboratory.

*Deceased.

II. EXPERIMENTAL OBSERVATIONS

Suspensions used in our experiments were purchased from Duke Scientific Corporation. The particles were made of polystyrene (density of 1.05 g/cm^3). Suspensions of these particles in water were stabilized by the manufacturer by adding trace amounts of an anionic surfactant and other unspecified additives (less than 0.5% by weight). Experiments were carried out for suspensions with mean diameters in the range of $1-70$ μm. The standard deviation in particle diameters for each suspension was less than 2% of the mean diameter. The volume fraction of the particles in suspensions obtained from the manufacturer was in the range of 0.002–0.018. A suspension of volume fraction lower than the one supplied by the manufacturer was prepared by adding de-ionized water. The experiments were carried out by evaporating suspensions at ambient temperature and humidity on either glass (Fisherbrand *Superfrost* disposable microscope slides from Fisher Scientific) or silicon substrate. The observed behaviors for both substrates were similar. Both substrates were pretreated to render them hydrophilic through a series of steps. First, the substrate was immersed in a 0.1*N* nitric acid for 5 min to remove the organic compounds from the surface. Next, the substrate was washed with de-ionized water and acetone. This was followed by immersing in a 15% hydrofluoric acid for 30 s, rinsing with de-ionized water, and drying.

A specified amount ($1.5-5$ μl) of a suspension drop was placed on the substrate. The drop quickly spread on the substrate and attained an approximately circular base within few seconds. The drop's extent along two mutually orthogonal directions was noted and a geometric mean of the two was taken. This mean will be referred to as the initial diameter of the deposited droplet. The evaporation process was recorded using a computer software (LOGITECH IMAGESTUDIO) that allowed recording of the evaporation process as a movie file using the option Create Animations.

Detailed observations for various particle sizes, volume fractions, and droplet radii are reported elsewhere (Su [12] and Liu [13]). Results for few representative cases are presented in Sec. IV where we compare the prediction of the theory with the experiments. Here, we summarize important observations. For suspensions containing 1 μm diameter particles, the experiments were carried out for particle volume fraction ϕ ranging from 0.000 25 to 0.005. In all cases the particles were advected by the liquid and formed rings near the edge of the drop. The contact line remained pinned throughout the evaporation process. For suspensions containing 3 μm diameter particles, a mixed behavior was observed with depinning observed only for the lowest volume fraction studied ($\phi=0.000\ 25$). The behavior for this smallest volume fraction case requires a more detailed discussion that we postpone until we derive the criterion in Sec. IV.

Figure 1 shows the case of a suspension of 3 μm diameter particles with $\phi=0.001$. For this case, the particles pin the contact line and form a ring close to the drop edge. We see two chains of particles. The drop edge is clearly visible in the figure. A particle arriving near the drop edge is seen to quickly move laterally toward one of the chains to increase the length of the chains. As more particles arrive at the drop edge, the two chains become longer and eventually merge into one. The particles at the end of the chains were seen to rotate around an axis normal to the substrate, indicating that they did not adhere firmly to the substrate. Interestingly, the position of the chain with respect to the drop edge remains quite steady as more particles arrive near the drop edge and the chains grow longer. Our theoretical calculation will explain why the distance between the row of the particles and the drop edge remains nearly constant.

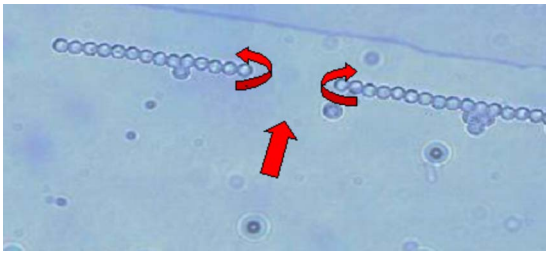

FIG. 1. (Color online) Formation of chains for a suspension of 3 μm diameter particles. The picture also shows a layer of liquid ahead of the particles and the rotating particles at the edge of the chains.

Experiments with all suspensions of particle diameters of 10 μm and greater showed that, after a brief initial outward motion toward the edge, the particles and the drop edge begin to move inward. Closer inspection revealed that the particles in these suspensions were nearly immobile presumably because they settled quickly to the substrate and strongly hindered their mobilities due to lubrication effects. The drop edge, being nearly devoid of particles, depinned and started moving inward. The receding drop edge must have caused the nearly immobile particles in its vicinity to protrude from the gas-liquid interface. The resulting capillary force on those protruded particles is strong enough to overcome the lubrication forces in the narrow gaps between the particles and the substrate so that the particles near the edge move quickly, aligning themselves parallel to the drop edge. Figure 2 shows images taken at various times during the evaporation of a suspension containing 25 μm diameter particles on a silicon substrate. We see that the particles away from the drop edge are nearly immobile even though there is considerable rearrangement of the particles near the receding drop edge.

We also carried out one experiment with a bidisperse drop containing a mixture of 50 μm diameter particles (volume fraction of 0.014) and 3 μm diameter particles (volume fraction of 0.005). For this case the smaller particles migrated toward the drop edge pinning the contact line while the larger particles migrated toward the center of the drop resulting in the segregation of the particles. Once again the larger particles were nearly immobile while the small particles were seen to migrate near the drop edge and pin the contact line. The decreasing volume of the liquid due to evaporation eventually must have caused the larger particles away from the center of the drop to begin protruding from the gas-liquid interface. The resulting capillary force must then be responsible for gradually moving the larger particles toward the drop center where they eventually formed a packed monolayer.

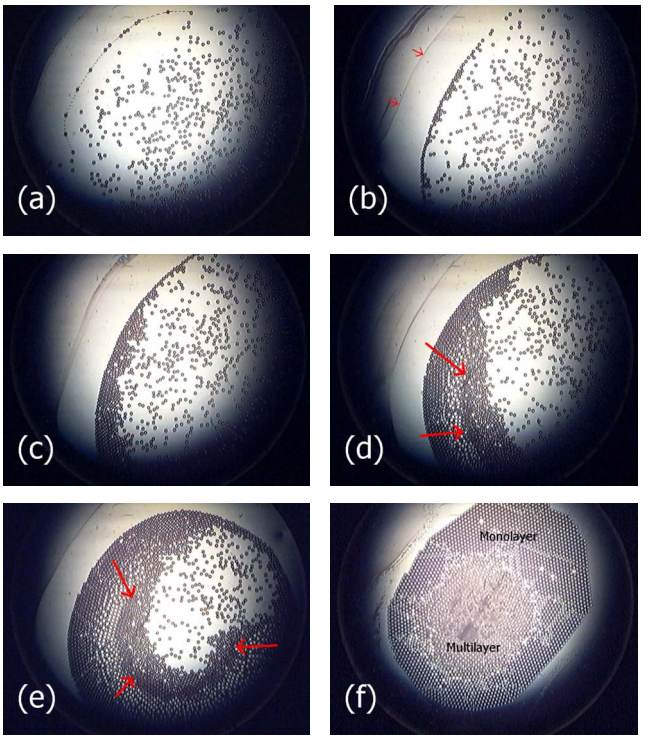

FIG. 2. (Color online) A sequence of events during the evaporation of a drop containing 25 μm diameter particles. The contact line steadily moves inward. Notice that only the particles near the drop edge rearrange and move inward as the drop edge moves toward the center. The final deposit consisted of nearly packed monolayer of particles surrounding a multilayer deposit.

In addition to the above, we also carried out experiments with drops of particle-free de-ionized water and the liquid withdrawn from the suspensions used in the above study to see what role the surfactant and other impurities present in the suspension may play in the evaporation process. Evaporation of the de-ionized water proceeded in two stages. During the first stage, which lasted about 1 min, the contact line remained pinned. During the second stage the contact line moved inward smoothly and the drop radius decreased smoothly with time. This duration was typically about 5 min long for a 1.5 μl de-ionized drop evaporating under ambient conditions at approximately 50% relative humidity. This time is approximately one-half to one-third the time typically taken for suspensions drops with the same volume. This two-stage behavior is consistent with a commonly accepted hypothesis that the contact angles for the advancing and receding drops are different. Behavior of the liquid withdrawn from the suspension, which contained surfactants and other additives, was different. The first stage of the pinned contact line, if present at all, was of very short duration. More interestingly, the drop edge did not remain smooth as the drop began to recede. Jetlike protrusions were seen emanating from the drop edge. As the time proceeded, this edge became rougher leaving a fractal-like deposit when the drop evaporation was complete. We believe that this results from an instability mechanism similar to the one seen during the spreading of surfactant drop and explained by Troian *et al.* [14]. The instability of the smooth circular shape of the receding drop edge, however, is not important in the analysis presented here that is primarily concerned with the problem of determining the capillary forces acting on the partially wetted particles near drop edge and the conditions under which the contact line remains pinned. Indeed, our experiments with suspensions of small particles did not show the instability typical of the particle-free liquid. Jetlike protrusions were seen only for large particle suspensions at relatively low humidity for which the contact line depins and moves rapidly inward.

III. CAPILLARY FORCES ON PARTICLES NEAR A DROP EDGE

Let us consider a drop resting on the surface of a substrate. We shall assume that the drop base in contact with the substrate is a circle of radius R. Let the contact angle at the gas-liquid-substrate contact line be denoted by θ_s. We shall be interested in the case when θ_s is small compared to unity, i.e., when the liquid-substrate interactions are favorable and the drop spreads well on the substrate. Let $h(x_1,x_2,t)$ represent the height of the liquid above the substrate at time t and (x_1,x_2) being the spatial coordinates in the plane of the substrate with the center of the circular drop base as the origin. The unit outward normal $\vec{n}$ at the gas-liquid interface is given by

$$\vec{n} = F[\vec{e}_3 - \vec{\nabla} h], \tag{1}$$

where $\vec{\nabla} = \vec{e}_1(\partial/\partial x_1) + \vec{e}_2(\partial/\partial x_2)$ is the gradient operator in the plane parallel to the substrate, $\vec{e}_k$ $(k=1,3)$ are the unit vectors along the coordinate axes, and $F^{-2} = 1 + |\vec{\nabla} h|^2$. The pressure inside a stationary drop is given by

$$p = p_a + \rho g(h - x_3) + \gamma \vec{\nabla} \cdot \vec{n}, \tag{2}$$

where p_a is the pressure outside the drop, ρ is the density of the liquid, g is the magnitude of the gravitational acceleration, and γ is the gas-liquid interfacial tension. Here, we have assumed that the gas density is negligibly small.

As noted by Deegan *et al.* [1], the rate of evaporation of the liquid from the gas-liquid interface can be determined by solving the diffusion equation for the water vapor in the gas phase. Since the time for water vapor to diffuse over a distance comparable to the drop radius R (about 2–4 mm) is much smaller than the time for the evaporation process in our experiments, the diffusion equation can be approximated by the quasisteady Laplace equation for the concentration of the water vapor in the space outside the drop. When the contact angle is small, the height of the drop is small compared to the radius, and, for the purpose of determining the mass flux of water vapor at the drop surface, the drop may be modeled as a thin disk to yield

$$\dot{m}_{ev} = \rho u_{ev} = \frac{\rho U_0 R}{(R^2 - r^2)^{1/2}}, \tag{3}$$

where $\dot{m}_{ev}$ is the evaporative mass flux, ρ is the density of liquid water, $r^2 = x_1^2 + x_2^2$, and

$$U_0 = \frac{2D_g(P^{sat} - P^v)M_w}{\pi\rho R R_g T}. \tag{4}$$

Here, D_g is the diffusivity of water vapor in the gas phase, P^{sat} is the vapor pressure of water at temperature T of the drop surface, P^v is the partial pressure of the water vapor in the ambient gas, M_w is the molecular weight of water, and R_g is the universal gas constant. We shall refer to U_0 as the characteristic evaporation velocity. It should be noted that the mass flux increases as r increases and becomes infinite at $r=R$. This, of course, is a consequence of assuming that the drop is infinitesimally thin. We note here that an expression for the evaporative mass flux has also been given for a spherical cap model of the drop by Popov [3]. His result, which is valid for arbitrary contact angles, agrees with the simple one presented here in the limit of vanishingly small contact angle.

When the contact line remains pinned we can use Eq. (3) to estimate the rate at which the volume of the drop will vary with time,

$$\frac{dV}{dt} = -2\pi R^2 U_0. \tag{5}$$

High evaporation rate near the pinned contact line causes a flow in the plane of the substrate with the magnitude of the velocity given by $O(U_0 R/h_0)$, where h_0 is the height of the drop at its center, i.e., at $r=0$. To drive this flow, a pressure gradient of magnitude $O(\mu U_0 R/h_0^3)$ must establish in the plane parallel to the substrate. This gradient, in turn, perturbs the shape of the stationary drop that can be estimated using Eq. (2) to be given by $h'/h_0 = O(\mathrm{Ca}R^4/h_0^4)$, where h' is the perturbation in the drop height from the stationary, nonevaporating, drop due to evaporation-induced viscous flow and

$$\mathrm{Ca} = \frac{\mu U_0}{\gamma} \tag{6}$$

is the capillary number representing the strength of viscous forces compared to the interfacial tension forces. For our experimental conditions, Ca is $O(10^{-8})$ while $R/h_0 = O(\theta_s)$ is $O(10^{-1})$. Thus, the effect of the evaporation-induced flow on the shape of the drop is negligible. Substituting for the unit normal vector from Eq. (1) into Eq. (2) and taking the gradient of the latter yield

$$\vec{\nabla}[\rho g h - \gamma \nabla^2 h] = 0, \tag{7}$$

with an error of $O(\mathrm{Ca}\theta_s^{-4})$ as explained above. Note also that we have also set F in Eq. (1) to unity. The error introduced in doing so is $O(\theta_s^2)$. We shall further simplify the problem of determining the drop shape by neglecting the gravitational term in the above equation. This is justified strictly when the Bond number $\rho g R^2/\gamma$ is small compared to unity. In our experiments, this number is actually comparable to unity as the drop radius was typically 2 mm. With $\rho = 1$ g/cm^3, $g = 981$ cm/s^2, and $\gamma = 30$ dyn/cm, the Bond number is about 2. Our primary interest here is in determining the effect of protruding particles, and the more relevant Bond number for that purpose is based on the radius a of the particles instead of the drop radius R. Since a/R in our experiments is very small, the neglect of the gravity term is justified as far as the shape perturbation caused by the protruding particle and the capillary force on the particle is concerned. Equation (7) therefore reduces to the much simpler Poisson equation,

$$\nabla^2 h + C(t) = 0, \tag{8}$$

where $C(t)$ is the integration constant.

When no particles are protruding from the gas-liquid interface, the drop shape is given by

$$h_\infty(\vec{r},t) = h_0(t)\left[1 - \frac{r^2}{R^2}\right]. \tag{9}$$

The initial value of the drop height, $h_0(0)$, is related to the contact angle at the three-phase contact line $r=R$ by

$$h_0(0) = (R/2)\tan\theta_s. \tag{10}$$

Since the volume of the drop is given by $V = \frac{1}{2}\pi h_0 R^2$, the rate at which the drop height varies is given by, using Eq. (5),

$$\frac{dh_0}{dt} = -4U_0. \tag{11}$$

In the absence of the particles, this will reduce the contact angle at the three-phase contact line and the drop will begin to recede. The outward radial flow of the liquid, however, carries the particles toward the drop edge until the particles almost touch the gas-liquid interface. We assume that a very thin liquid film sandwiched between the particle surface and the gas-liquid interface will drain away so that the hydrodynamic force acting on the particles pushing them toward the drop edge will force the particles to become partially dewetted and the particles will begin to protrude from the gas-liquid interface. This protrusion will eventually lead to a capillary force on the particles that will balance the hydrodynamic force and arrest the further outward motion of the particles. Determining this equilibrium position and the effect of these protruding particles on the contact line angle at the substrate is the primary purpose of the present analysis.

Let us therefore consider the effect of protruding particles. The experiments showed that the particles' motion is arrested at approximately the same radial position from the drop center. We therefore consider N particles protruding with their centers at (r_0, θ_n, a), $n = 1, 2, \ldots, N$. The cylindrical coordinates used here are related to the Cartesian coordinates introduced earlier by $x_1 = r\cos\theta$, $x_2 = r\sin\theta$, and $x_3 = z$. We have examined a number of problems including a single particle, a pair of particles, a chain of touching particles, and the equispaced particles [12]. To our surprise, the radial component of the capillary force as a function of r_0 varied very little among all the examined cases. On the other hand, this is consistent with the experimental observations that the radial position of the protruding particles does not appear to change as additional particles advected by the fluid begin to protrude. We shall present here the analysis for the case of equispaced particles for which

$$\theta_n = 2\pi(n-1)/N, \quad n = 1, 2, \ldots, N. \tag{12}$$

To determine the capillary force on the particles one must first determine the position of the contact line on each of the protruding particles. For the case of equispaced particles, it will suffice to consider a representative particle, $n=1$, with its center along the x_1 axis. Let θ_p denote the contact angle for the line separating the particle, liquid, and gas phases. We require that along this contact line,

$$\vec{n} \cdot \vec{n}_p = \cos\ \theta_p, \tag{13}$$

where $\vec{n}_p$ is the unit outward normal on the surface of the particle. We introduce a cylindrical coordinate system (σ, φ, z) passing through the center of the particle such that

$$x_1 = r_0 + \sigma \cos\ \varphi, \quad x_2 = \sigma \sin\ \varphi, \quad \text{and} \quad x_3 = z. \tag{14}$$

Let $\sigma=\sigma_c(\varphi)$ describe the contact line at the particle surface. Using

$$\vec{n}_p = [(z-a)\vec{e}_z + \sigma_c \vec{e}_\sigma]/a, \tag{15}$$

$\vec{e}_z$ and $\vec{e}_\sigma$ being the unit vectors in the particle-centered cylindrical coordinate system, and Eq. (1) for the unit outward normal at the gas-liquid interface, Eq. (13) reduces to

$$h - \sigma \frac{\partial h}{\partial \sigma} = a[1 + \cos\ \theta_p] \quad \text{at} \quad \sigma = \sigma_c(\varphi). \tag{16}$$

Since the contact line must also lie on the surface of the particle, we have an additional condition,

$$h = a + (a^2 - \sigma^2)^{1/2} \quad \text{at} \quad \sigma = \sigma_c(\varphi). \tag{17}$$

The positive sign on the right-hand side of the above equation assumes that less than half of the particle is protruding from the gas-liquid interface.

Instead of prescribing similar two conditions for the contact line at the substrate, we shall assume that the gas-liquid-substrate contact line remains circular and pinned. Thus, we require

$$h = 0 \quad \text{at} \quad r = R. \tag{18}$$

We shall determine the contact angle at the drop edge once the drop shape is determined to derive a condition under which the assumption of pinned contact line is justified in Sec. IV.

We have developed two methods for solving the problem described by Eqs. (8) and (16)–(18). One method, referred to as method A, is described below while the second one, referred to as method B, is described in Appendix C.

Method A

In this method, we assume that the gas-liquid-particle contact line is given by

$$\sigma_c(\varphi) = \sigma_0 + \sigma'(\varphi) \quad \text{with} \quad |\sigma'| \ll \sigma_0, \tag{19}$$

where σ_0 is independent of the polar angle φ. In other words, we assume that the contact line to leading order is a circle in a plane parallel to the substrate. We shall examine the conditions under which this approximation is justified later in the section. Method B described in Appendix C is more general in that it allows the approximate plane of the contact line to be at an arbitrary angle to the normal to the substrate.

Substituting Eq. (19) into Eqs. (16) and (17) we obtain

$$\left[h - \sigma \frac{\partial h}{\partial \sigma}\right]_{\sigma=\sigma_0} - \sigma' \sigma_0 \left[\frac{\partial^2 h}{\partial \sigma^2}\right]_{\sigma=\sigma_0} + O(\sigma'^2/a) = a[1 + \cos\ \theta_p], \tag{20}$$

$$\left[h + \sigma' \frac{\partial h}{\partial \sigma}\right]_{\sigma=\sigma_0} = a + (a^2 - \sigma_0^2)^{1/2} - \frac{\sigma_0 \sigma'}{(a^2 - \sigma_0^2)^{1/2}} + O(\sigma'^2/a). \tag{21}$$

We shall use the method of multipole expansions [15] to determine h, σ_0, and σ'. Accordingly, we write

$$h(\vec{r}, t) = h_\infty(\vec{r}, t) + \sum_{n=0}^{\infty} (-1)^n A_n \frac{\partial^n}{\partial r_0^n} G(\vec{r} - \vec{r}_0), \tag{22}$$

where $\vec{r}_0 = r_0 \vec{e}_r$, A_n are the coefficients of the multipoles aligned along the radial direction, and G is the Green's function satisfying

$$\nabla^2 G(\vec{r} - \vec{r}_0) + B = \frac{2\pi}{r_0} \sum_{n=1}^{N} \delta(r - r_0)\, \delta(\theta - \theta_n), \tag{23}$$

$$G = 0 \quad \text{at} \quad r = R, \tag{24}$$

$$\int_{r=0}^{R} \int_{\theta=0}^{2\pi} rG\, dr\, d\theta = 0. \tag{25}$$

Physically, G represents the solution of a two-dimensional heat conduction problem with N heat sinks uniformly distributed along the circle $r=r_0$ with the temperature at $r=R$ maintained at a constant value equal to zero. In addition, a source of strength B is distributed throughout $0<r<R$ so that the average value of G over the circle is zero. It may be noted that G and its derivatives satisfy the differential equation [Eq. (8)] and the boundary condition [Eq. (18)], and therefore Eq. (22) represents a general solution for h. The first term on the right-hand side of Eq. (22) represents the drop height in the absence of the protruding particles, while the second term represents the effect of the protruding particles. Condition (25) is necessary in order to ensure that the total volume of the liquid remains unchanged when the particles protrude from the gas-liquid interface. Note also that Eq. (23) renders G a periodic function of θ with a period $2\pi/N$. An expression for G is given in Appendix A.

The multipole coefficients A_n and the contact line variables σ_0 and σ' must be determined by satisfying the conditions [Eqs. (20) and (21)] at the contact line. Since G is a periodic function of θ, it will suffice to determine these conditions on a representative particle placed on the x_1 axis. For this purpose, we expand h in the cylindrical coordinate system with its axis passing through the center of the particle at $\vec{r}_0 = r_0 \vec{e}_1$. Noting that $G = \ln \sigma + G^r$, where G^r is the regular part of G near $\vec{r} = \vec{r}_0$ (Appendix A), h may be expressed as (Sangani and Yao [15])

$$h = \sum_{n=0}^{\infty} f_n(\sigma)\cos n\varphi, \tag{26}$$

with

$$f_0 = A_0 \ln \sigma + E_0 - s\sigma^2, \tag{27}$$

$$f_n = (-1)^{n-1}(n-1)!\, A_n\sigma^{-n} + E_n\sigma^n, \quad n \geq 1. \tag{28}$$

Here, $s=(C+A_0B)/4$ and

$$E_n = \frac{1}{n!}\sum_{m=0}^{\infty}(-1)^{n+m}A_m\frac{\partial^{m+n}G^r}{\partial r_0^{m+n}} + \delta_{n0}h_\infty(r_0,t) - 2Cr_0\delta_{n1}, \tag{29}$$

where the derivatives of G^r are to be evaluated at $\vec{r}=r_0\vec{e}_1$. An expression for G^r is given in Appendix A. As shown there,

$$g_0 \equiv G^r(r_0,r_0) = \ln\left[\frac{NR^Nr_0^{N-1}}{R^{2N}-r_0^{2N}}\right] + N\left(1-\frac{r_0^2}{R^2}\right)^2, \tag{30}$$

$$g_1 \equiv -\left[\frac{\partial G^r(\vec{r},r_0)}{\partial r_0}\right]_{\vec{r}=r_0\vec{e}_1} = \frac{N-1}{2r_0} + \frac{Nr_0^{2N-1}}{R^{2N}-r_0^{2N}} - \frac{2Nr_0}{R^2}\left(1-\frac{r_0^2}{R^2}\right). \tag{31}$$

It may be noted that for $\delta \equiv R-r_0 \ll R$, $g_0=O(\ln \delta)$ and $g_1=O(1/\delta)$. In general, the nth derivative of G^r is $O(\delta^{-n})$.

The particles protrude from the gas-liquid interface at a location where the drop height is comparable to the diameter of the particles. Therefore, $\delta \equiv R-r_0=O(a/\theta_s)$. We shall be interested in the case $\delta \ll R$. This condition is satisfied when $h_0(t) \gg a$. For this case, it can be shown that $G^r=O(\ln \delta)$ and $\partial^n G^r/\partial r_0^n=O(\delta^{-n})$, $n \geq 1$. Substituting these orders of magnitude estimates in Eqs. (28) and (29), we find that $E_n=A_0[O(\delta^{-n})]$ and $f_n=A_0O[(\sigma_0/\delta)^n]$. Next, we expand σ' as given by

$$\sigma' = \sum_{n=1}^{\infty}\sigma_n\cos n\varphi \tag{32}$$

and substitute it into Eqs. (20) and (21) to find that $\sigma_n/\sigma_0=O[(\sigma_0/\delta)^n]$. Considering only the terms up to $n=1$ we obtain

$$2A_1 = -\sigma_1[A_0 + 2s\sigma_0^2], \tag{33}$$

$$E_1\sigma_0 + (\sigma_1/\sigma_0)[A_0/2 - 3s\sigma_0^2 + \sigma_0^2/(a^2-\sigma_0^2)^{1/2}] = 0, \tag{34}$$

$$A_0[\ln \sigma_0 - 1] + s\sigma_0^2 + E_0 = a[1+\cos\theta_p], \tag{35}$$

$$A_0 \ln \sigma_0 + E_0 - s\sigma_0^2 = a + (a^2-\sigma_0^2)^{1/2}. \tag{36}$$

The above four equations, together with Eq. (29), which expresses E_0 and E_1 in terms of A_0 and A_1, can be solved for the four unknowns, A_0, A_1, σ_0, and σ_1. These equations can be further simplified with slight loss in accuracy by setting $s=0$ (error of $O[(a/R)\theta_s]$) and neglecting terms involving second derivatives of G^r in evaluating E_1 [error of $O(\theta_s^2)$].

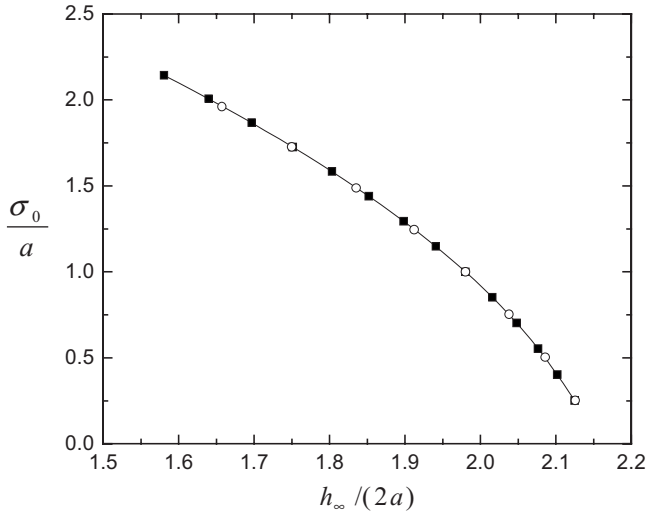

FIG. 3. Contact line radius σ_0 as a function of undisturbed liquid height h_∞ for three cases: (i) $N=1$, $a=0.5$ μm (solid line); (ii) $N=1$, $a=5$ μm (squares); and (iii) $N=100$, $a=0.5$ μm (open circles). For all three cases $R=2$ mm, $\theta_p=0.2$, and $\theta_s=0.1$.

The resulting simplified equations take the form

$$A_0 = a(\cos\theta_0 - \cos\theta_p), \tag{37}$$

$$\sigma_1 = \frac{-\sigma_0(h'_\infty + A_0g_1)}{A_0/(2\sigma_0) + \tan\theta_0}, \tag{38}$$

$$A_1 = -(\sigma_1/2)A_0, \tag{39}$$

$$h_\infty = a(1+\cos\theta_0) - A_0(\ln\sigma_0 + g_0) + A_1g_1. \tag{40}$$

Here, θ_0 is defined by $\sigma_0=a\sin\theta_0$, h_∞ is evaluated at $r=r_0$, and h'_∞ is the derivative of h_∞ with r at $r=r_0$. The above equations can be used to evaluate σ_0, σ_1, and A_0 as functions of r_0.

The force on the particles can be decomposed into three parts. The first is the force due to interfacial tension acting along the gas-liquid-particle contact line. The second is the force due to uneven pressure distribution on the surface of the particle with the pressure in the liquid being greater than in the gas by $\gamma\vec{\nabla}\cdot\vec{n}=-\gamma\nabla^2h=4\gamma s$. Here, $s=(C+A_0B)/4$ as defined earlier. Note that $C=4h_0(0)/R^2=O(\theta_s/R)$. Finally, the third is the hydrodynamic force. We shall propose an expression for determining the last part in Sec. IV. Expressions for determining the first two are given in Appendix B.

The nonlinear set consisting of Eqs. (37)–(40) can be solved to determine the four quantities σ_1, A_0, A_1, and h_∞ as functions of σ_0. Note that these equations also contain r_0, which is related to h_∞ by $h_\infty=h_0(1-r_0^2/R^2)$. We used a MATLAB-based iterative method to determine these quantities as functions of σ_0.

The nondimensional parameters governing the problem are the contact angles at the particle and substrate surfaces given, respectively, by θ_p and θ_s and the ratio of the particle to the deposited drop radius, a/R. Figure 3 shows the contact line radius σ_0 as a function of h_∞ for two different values of R/a. These two values correspond to our experiments in

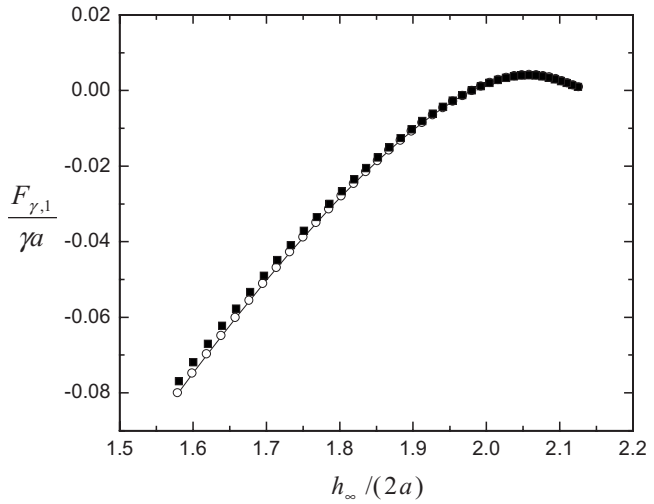

FIG. 4. Capillary force as a function of undisturbed liquid height h_∞ for three cases: (i) $N=1$, $a=0.5$ μm (solid line); (ii) $N=1$, $a=5$ μm (squares); and (iii) $N=100$, $a=0.5$ μm (open circles). For all three cases $R=2$ mm, $\theta_p=0.2$, and $\theta_s=0.1$.

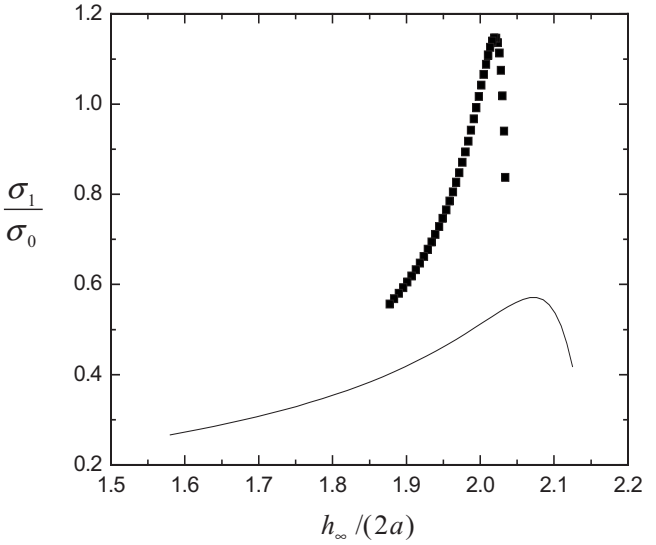

FIG. 5. σ_1/σ_0 as a function of $h_\infty/(2a)$ for two cases: (i) $\theta_p=0.2$, $\theta_s=0.1$ (solid line); (ii) $\theta_p=0.1$, $\theta_s=0.1$ (squares). $N=1$, $a=0.5$ μm, and $R=2$ mm in both cases.

which R was approximately 2 mm and the particle diameters were 1 and 10 μm. Note that since h_∞ is a function of r_0, σ_0 as a function of the radial position r_0 of the particle can, in principle, be obtained from the results for σ_0 plotted against h_∞. A particle advected by the liquid will first protrude from the gas-liquid interface at the radial position r_0 such that $h_\infty(r_0)/a=2$. The contact line radius is finite for this radial position. As the particle travels further out, h_∞ decreases and the gas-liquid-particle contact line radius increases. If, on the other hand, the particle moves inward, the contact line decreases and remains nonzero even for radial positions with $h_\infty/a>2$. Also shown in Fig. 3 are the results for the case when N, the number of particles along the circle $r=r_0$, is 100 and the particle diameter is 1 μm. We see that the results for all three cases are indistinguishable from each other. In doing these computations we have set G_v in Eq. (A1), which represents the effect of the protruding particles on the total volume of the liquid in the drop, to zero. In an actual process, h_∞ decreases with time at given r_0 while the number of particles N at the drop edge increases. Setting $G_v=0$ and $h_\infty(r_0,t)=h_\infty(r_0,0)$ should provide a reasonable approximation to what will happen in the dynamic process.

Figure 4 shows the capillary force as a function of h_∞. Since the capillary number $\mu U_0/\gamma$ is very small, the motion of the particles protruding from the gas-liquid interface is largely determined by the magnitude of the capillary force. We see that the capillary force is positive at $h_\infty=2a$, suggesting thereby that the particle experiences a radial force pushing it outward toward the drop edge. As the particle travels further out, the force decreases and vanishes when h_∞ is approximately equal to $1.98a$. The force turns negative for smaller h_∞ so that the equilibrium position of the particles corresponds roughly to the above mentioned value of h_∞. Figure 4 shows results for two different particle radii and for $N=1$ and $N=100$. Once again, we see that the results for the three cases are essentially indistinguishable from each other.

The result that the equilibrium position of the particles is nearly independent of the number of particles at the drop edge is somewhat surprising but consistent with the experimental observations (cf. Fig. 1) that showed that as more particles arrive at the drop edge the radial positions of the other protruding particles do not change. Also, the result that the curve is nearly independent of a/R is very interesting as it suggests that it is not possible to explain the observation that the small particles pin the contact line while the large particles do not on the basis of capillary force behavior for small and large particles.

Our analysis assumed that the gas-liquid-particle contact line is nearly circular, i.e., $|\sigma_1| \ll \sigma_0$. We can now check how well this assumption is justified. Figure 5 shows σ_1/σ_0 as a function of h_∞/a for two selected combinations of θ_p and θ_s. We find that, in general, this is not a good approximation. In fact, when $\theta_s>\theta_p$, the magnitude of σ_1 exceeds that of σ_0 for some values of h_∞. It appears that the assumption that the contact line to leading order is circular and in the plane parallel to the substrate is justified only when θ_p is significantly greater than θ_s. In Appendix C, we present an alternate model in which the contact line plane is allowed to incline at an arbitrary angle to the substrate. Although this model is more accurate and predicts interesting behavior, the simpler analysis presented in this section is adequate for deriving the principal result of the present study, i.e., the criterion for conditions under which the particles will aid in pinning the contact line.

IV. CRITERION FOR THE CONTACT LINE PINNING

Our experimental observations suggest that smaller particles tend to form rings at the drop edge while larger particles tend to move toward the center of the drop dragging with them the drop edge. Since the force versus radial position curves for small and large particles are essentially the same, the above observation cannot be explained solely on the basis of the capillary force on the particles. For example,

we showed that the radial position r_0 of the particles is approximately given by $h_\infty(r_0)=1.98a$. This will correspond approximately to $\delta=R-r_0=0.99aR/h_0(t)$, where $h_0(t)$ is the height of the drop at $r=0$. As $h_0(t)$ decreases with time due to evaporation, this would suggest that the distance between the particle and the drop edge will increase. This, however, is not observed generally. An exception is the case of a mixture of 50 and 3 μm diameter particles where the distance between the drop edge and the 50 μm diameter particles increases with time. Thus, the migration of the larger particles toward the center of the drop in the bidisperse suspension that are pinned by the smaller may be explained by saying that the equilibrium position of the larger protruding particles continues to shift toward the center of the drop as the drop height decreases. Since δ is observed to remain nearly constant in most monodisperse suspension cases, the pinning/depinning phenomenon must be related to the effect of the particles on the contact angle at the drop edge.

We therefore examine how the particles protruding from the gas-liquid interface affects the gas-liquid-substrate contact line. Our analysis so far has assumed that the drop edge is smooth and circular and pinned at $r=R$. This violates, in general, the condition that the angle made by the drop at the drop edge should equal the contact angle for the gas-liquid-substrate system. Particles arriving near the drop edge will increase the contact angle while the evaporation will decrease it. If the former effect is large enough then the drop might spread further somewhat but the particles will eventually aid in pinning the contact line, and our assumption of the drop edge being pinned will be justified *a posteriori.* Our goal is to make a number of reasonable approximations to derive a relatively simple criterion for pinning the contact line. The steps include determining the increase in the contact angle caused by a single particle that is in equilibrium under the influence of capillary and hydrodynamic forces and determining the rate at which the new particles arrive near the drop edge.

For a single particle placed at $r=r_0=R-\delta$ on the x_1 axis ($\theta=0$), the effect of the particle on the contact line angle is the greatest at a point on the x_1 axis and $r=R$. The contribution to the tangent of the contact angle at the substrate, neglecting the higher-order multipoles and assuming that $\delta \ll R$, is given by $-2A_0/\delta$. (This corresponds to a monopole A_0 and an image monopole $-A_0$ on the other side of the drop edge.) The next particle to protrude from the gas-liquid interface in its vicinity will be immediately attracted to it because of the strong attractive capillary forces, and together both particles will contribute $-4A_0/\delta$ to the tangent of contact angle. If n_c is the number of chains formed around the drop circumference when a total of N particles is protruding, then the angular-averaged contact angle is given by

$$\langle \tan\theta_s(t)\rangle = -\left[\left(\frac{\partial h_\infty}{\partial r}\right)(R,t) + \frac{2NA_0}{n_c\delta}\right]. \tag{41}$$

The first term on the right-hand side is the contribution from the undisturbed shape of the drop whose height is decreasing because of the evaporation and the second is the leading-order contribution from the protruding particles. The number of chains n_c remains O(1) and generally decreases with time as more particles arrive at the drop edge and some of the chains coalesce as described in Sec. II (cf. Fig. 1).

In order that the contact line remains pinned, $\langle\theta_s\rangle$ must not decrease as the evaporation proceeds. The first term on the right-hand side of the above equation can be related to the rate of evaporation using Eqs. (9) and (11) that yield

$$-\left(\frac{\partial h_\infty}{\partial r}\right)_{r=R} = 2h_0(t)/R = 2h_0(0)/R - 8U_0t/R = \theta_s(0) - 8U_0t/R, \tag{42}$$

indicating that the effect of the evaporation is to reduce the contact angle with time. We have assumed that the contact angle is small and, hence, $\tan\theta_s \approx \theta_s$. In order that the particles pin the contact line, the negative term on the right-hand side of the second equality in the above expression must be balanced by the second term on the right-hand side of Eq. (41). However, when the capillary force is zero, the monopole A_0 also vanishes, and the contribution from the protruding particles to the contact angle vanishes. To obtain a nonzero estimate of A_0 and hence the effect of the particles on the contact angle, we must use the fact that the capillary force is small but nonzero as it must be balanced by the hydrodynamic force on the particle. Thus, we need an estimate of the drag force. Since the Reynolds number of the flow is small, the drag on a particle is given by

$$F_h = 6\pi\mu a[\lambda U_r - \lambda_m dr_0/dt], \tag{43}$$

where μ is the viscosity of the liquid, λ is the drag coefficient for a particle placed in a film through which there is a mean liquid flow, λ_m is the drag coefficient for a particle moving through a quiescent liquid film, and U_r is the average undisturbed radial velocity of the fluid at $r=r_0$. Estimates of the drag coefficients are given later in Sec. IV A. The average radial velocity can be estimated using

$$U_r = \frac{q(r_0)}{2\pi r h_\infty(r_0)} = \frac{U_0R^2}{r_0h_\infty(r_0)}[(1-r_0^2/R^2)^{1/2} - (1-r_0^2/R^2)^2], \tag{44}$$

where $q(r_0)$ is the evaporation-induced volumetric flow rate of the liquid through a cylindrical surface of radius r_0 and height $h_\infty(r_0)$. The first term on the extreme right-hand side of the above expression accounts for the liquid evaporation from $r=r_0$ to $r=R$, while the second term corresponds to the decrease in the volume of liquid for same values of r. For small particles, the radial position of the particles is close to R so that the last term in the above expression may be neglected. Taking $h_\infty \approx 2a$, the above expression simplifies to an approximate relation (for $\delta=R-r_0 \ll R$),

$$U_r = \frac{U_0}{2^{1/2}}\left(\frac{R}{a}\right)\left(\frac{a}{h_0}\right)^{1/2}, \tag{45}$$

where the use has been made of the relation $(2a)/(R-r_0) \approx (2h_0)/R_s$, both being equal to the contact angle θ_s. This equation suggests that the smaller particles, being closer to the drop edge, experience larger relative velocity.

The viscous drag force given by Eqs. (43) and (45) must be balanced by the capillary force pulling the particle toward the drop center. For a fixed protruding particle, $dr_0/dt=0$ and the capillary force must equal the drag force. Thus,

$$\frac{F_\gamma}{\gamma a} = -\frac{F_h}{\gamma a} - \frac{\mu U_0}{\gamma}\left(\frac{6\pi\lambda}{2^{1/2}}\right)\left(\frac{R}{a}\right)\left(\frac{a}{h_0}\right)^{1/2}. \tag{46}$$

To determine A_0 corresponding to this force, we note that when $\mathrm{Ca}=\mu U_0/\gamma$ is very small, θ_0 must be close to θ_p [cf. Eq. (B6)]. Let

$$\theta_0 = \theta_p + \varepsilon \quad \text{with} \quad \varepsilon \ll 1. \tag{47}$$

For this limiting case, the contact line is in a plane nearly parallel to the substrate, and according to the analysis presented in Sec. III,

$$A_0 \approx -\varepsilon a \sin\theta_p \tag{48}$$

and

$$\frac{F_\gamma}{\gamma a} = 2\pi\varepsilon \sin\theta_p h'_\infty, \tag{49}$$

where $h'_\infty=(\partial h_\infty/\partial r)_{r=r_0}$. Equating the above expression for the capillary force to that required to overcome the viscous drag force [cf. Eq. (46)], we obtain an estimate for ε, which, upon substitution into Eq. (48), yields

$$A_0 = a\mathrm{Ca}\frac{3\lambda}{2^{1/2}h'_\infty}\left(\frac{R}{a}\right)\left(\frac{a}{h_0}\right)^{1/2}. \tag{50}$$

This shows that, to leading order, the monopole A_0 is proportional to the capillary number. The derivative of h_∞ required in the above expression varies with time. We shall use the initial value $[-2h_0(0)r_0/R^2 \approx -2h_0(0)/R]$. This will underestimate the magnitude of A_0 and hence the effect of the particles on the contact line angle as $h_0(t)$ decreases with time. On the other hand, the use of δ in the denominator of the right-hand side of Eq. (41) overestimates the effect of the particles when the particle chain length becomes comparable or greater than δ. The number of particles at the drop edge can be obtained from the radial flow rate as given by

$$N = \frac{3\phi t q(r_0)}{4\pi a^3} = \frac{3\phi t U_0}{2^{1/2}a}\left(\frac{R}{a}\right)^{3/2}\left(\frac{R}{h_0}\right)^{1/2}, \tag{51}$$

where ϕ is the volume fraction of the particles. In obtaining the second equality, we have related q to the average radial velocity U_r and used the approximate relation [Eq. (45)] for the latter. Note also that we have assumed that the mean particle velocity is the same as the fluid velocity and that no particles have settled out. Substituting for A_0 and N into Eq. (41), and rearranging, we obtain

$$\langle \tan\theta_s(t)\rangle = \tan\theta_s(0) - \frac{8U_0 t}{R}\left[1 - \frac{9\lambda}{16 n_c}\frac{R^4}{a^3 h_0}C_a\phi\right]. \tag{52}$$

The first term inside the square brackets represents the effect of the decreasing volume of the drop due to evaporation, while the second term represents the effect of the particles protruding the gas-liquid interface near the drop edge. In order that the contact line remains pinned, the contact angle must not decrease with time. This requires that the term inside the square brackets is negative or

$$\Psi \equiv \phi C_a \frac{R^4}{a^3 h_0} \geq C \equiv \frac{16}{9\lambda n_c}, \tag{53}$$

indicating that larger volume fraction, smaller contact angle at the substrate (large R/h_0), larger drop volume, and smaller particle radius favor the contact line pinning.

A. Hydrodynamic drag coefficient

We now briefly digress and summarize some relevant results for the drag on a particle or a raw of particles in a film. Recently, Ozarkar and Sangani [17] examined the problem of determining the drag on a spherical particle resting on a substrate in a film of height equal to the diameter of the particle. The gas-liquid interface was nondeformable and stress-free. The liquid flow far from the particle was assumed to be parabolic with mean velocity U. The drag force was found to be about 1.9 times the Stokes drag for this case. These authors also gave an estimate of the drag coefficient λ_m on a particle moving through a thin liquid film. This coefficient diverges logarithmically as the gap between the particle and the substrate becomes vanishingly small due to lubrication effects. When the particle and the substrate are rough, one may equate the gap to the roughness (Smart *et al.* [18,19]) to estimate the sliding velocity of a particle in a film. The drag on a chain of small number of touching fixed particles in a film has also been computed by Ozarkar [20], who found that the drag per particle is smaller than for a single particle as the fluid flows mostly around the chain of particles. The drag will be dramatically higher, however, when the chain length becomes large enough so that the fluid is forced to flow through the gap between the particles. This will be the situation in the present case when the particle chain length becomes larger than δ, the distance between the particles and the drop edge. The results for this case are not available at present but the case of an infinitely long chain of touching particles sandwiched between two stress-free boundaries has been examined by Sangani and Behl [21] who found that the drag on a particle in such an array is about 40 times the Stokes drag. For two staggered rows of particles placed in the flow, the drag coefficient rises to about 160.

In the present case of a fixed protruding particle, the drag is expected to be higher that computed by Ozarkar and Sangani, but in the absence of a more accurate estimate, we shall take $\lambda=1.9$, result corresponding to a single particle in a film of same height as the particle diameter. This yields $C=0.94/n_c$.

B. Comparison with experiments

We now compare the criterion given by Eq. (53) with the experimental observations. Table I gives the experimental data for suspensions at various particle radii and volume fractions and the computed values of Ψ. The radius of the deposited suspension drop was determined after the evapo-

TABLE I. Pinning/depinning behavior of suspensions for various particle diameters, drop volumes, and particle volume fractions.

$2a$ (μm)	V (μl)	H	ϕ	R_s (mm)	R (mm)	h_0 (μm)	U_0 (cm/s)	t_{expt} (min)	t_{est} (min)	t^*_{ring}	Ψ	Pin (p)/ depin (d)
1	1.5	0.53	5×10^{-3}	2.4	3.2	91	5.4×10^{-6}	9.7	8.5	3×10^{-3}	109	p
1	1.5	0.62	1×10^{-3}	1.9	3.5	80	4.1×10^{-6}	16.5	9.8	2×10^{-2}	24.1	p
1	1.5	0.59	5×10^{-4}	1.8	3.4	84	4.5×10^{-6}	14.6	9.3	3×10^{-3}	11.7	p
1	1.5	0.68	2.5×10^{-4}	1.9	3.6	74	3.3×10^{-6}	17.9	11.2	7×10^{-2}	6.2	p
1	3.0	0.62	5×10^{-3}	2.9	3.9	126	3.6×10^{-6}	19.2	17.4	2×10^{-3}	111	p
1	3.0	0.60	1×10^{-3}	2.1	3.8	132	3.9×10^{-6}	22.4	16.9	1×10^{-2}	20.5	p
1	3.0	0.68	5×10^{-4}	2.1	4.0	119	3.0×10^{-6}	29.4	20.1	2×10^{-2}	10.6	p
1	3.0	0.60	2.5×10^{-4}	2.3	3.8	132	3.9×10^{-6}	19.6	16.9	5×10^{-2}	5.1	p
3	1.5	0.62	1×10^{-3}	2.5	3.5	80	4.1×10^{-6}	19.2	9.8	9×10^{-2}	0.89	p
3	1.5	0.65	5×10^{-4}	2.8	3.5	78	3.7×10^{-6}	18.7	10.5	0.18	0.44	p
3	1.5	0.53	2.5×10^{-4}	2.8	3.2	91	5.4×10^{-6}	10.9	8.5	0.35	0.20	d/p
3	3.0	0.62	1×10^{-3}	2.1	3.9	126	3.6×10^{-6}	23.4	17.4	0.06	0.82	p
3	3.0	0.65	5×10^{-4}	2.1	4.0	119	3.3×10^{-6}	25.2	18.4	0.12	0.43	p
3	3.0	0.54	2.5×10^{-4}	2.2	3.6	147	4.8×10^{-6}	15.4	15.5	0.25	0.17	d
3	5.0	0.62	1×10^{-3}	2.5	4.5	157	3.1×10^{-6}	31.4	25.1	0.05	1.01	p
3	5.0	0.65	5×10^{-4}	2.8	4.6	150	2.8×10^{-6}	33.5	26.6	0.10	0.52	p
3	5.0	0.53	2.5×10^{-4}	2.8	4.3	172	4.1×10^{-6}	27.4	21.2	0.19	0.25	d/p
10	5.0	0.56	0.01	4.3	2.9	172	3.8×10^{-6}	33.6	24.0	0.03	0.25	d

ration was complete by examining the outer boundary of the residue left on the substrate. A geometric mean of the maximum extent of the residue along two mutually perpendicular directions divided by two was taken to be the radius of the deposited drop. The radius thus determined is denoted by R_s. Also shown in the table is the radius R of a droplet of same volume of liquid free of particles. The latter is a function of the ambient humidity and drop volume, while the former also depends on the radius of the particles and their volume fractions. Note that R_s is significantly smaller than R. The spreading of the suspension drop placed on the substrate is arrested by one of the two mechanisms: (i) the particles advected by the fluid and arriving near the drop edge will begin to pin the contact line before the drop had the chance to fully spread or (ii) the particles settle to the substrate and induce drag on the spreading liquid slowing thereby its spread. Since there is no simple theory to predict R_s given the drop volume, particle radius, and volume fraction, we used R for estimating Ψ. We also took $\mu=0.01$ g/cm s and $\gamma=20$ dyn/cm in all cases.

The initial height h_0 of the drop was estimated using $h_0(0)=2V/(\pi R^2)$, where V is the volume of the drop. The characteristic evaporation velocity U_0 was estimated using Eq. (4). The diffusivity of water vapor in air was estimated using $D_g=0.223(T/273)^{1.5}$ cm^2/s. The temperature was taken to be equal to 295 K. The time for the evaporation to complete is also given in Table I. When the drop remains pinned, this time can be related to the characteristic evaporation velocity by

$$t_{est}=\frac{h_0(0)}{4U_0}. \tag{54}$$

As seen in Table I, the estimates obtained are somewhat lower than the experimentally determined values. On the other hand, if we had used R_s instead of R, to estimate U_0, and, hence, the evaporation time, then we would have obtained estimates for the evaporation times that are greater than the experimental values. (Note that U_0 is inversely proportional to the radius of the drop while h_0 is inversely proportional to the square of the radius.) At any rate, the time estimates are generally comparable and the agreement with the experiments may be regarded as quite satisfactory.

As mentioned in Sec. II, we carried out experiments with particles of diameters 1, 3, 10, 15, 25, 50, and 70 μm at three to four different volume fractions and for two to three different drop volumes. Due to space limitations, Table I presents the data for the most relevant cases. More detailed data are presented by Liu [13]. The suspensions of 1 μm diameter particles pinned the contact line in all the cases examined, whereas the particles of 10 μm diameter or greater migrated toward the center of the drop. As mentioned in Sec. II, the density difference between the particles and the liquid ($\Delta\rho=0.05$ g/cm^3) was not small enough to keep the particles of 10 μm diameter or greater from settling out, and therefore the data for these suspensions are not relevant to the present study. The data for the case of 3 μm diameter suspensions are perhaps the most interesting. The suspensions with $\phi=0.000\,25$ showed the depinning behavior while the higher volume fractions showed pinning.

Of the three drop volumes examined for $\phi=0.000\,25$, the case that exhibited the best example of depinning corresponded to the drop of volume 3 μl. For 1.5 and 5 μl volume drops, the contact line remained pinned for a considerable duration with the distance between the particle chain and the drop edge (δ) slowly increasing during this period. In other words, only the particle chains were moving inward. Note that if the contact line is pinned then the equilibrium position r_0 of the particle is given by $h_\infty(r_0,t)\approx 1.98a$. This

corresponds to $\delta \approx 0.99aR/h_0(t)$, so that δ will increase with time as $h_0(t)$ decreases due to evaporation. This suggests that for considerable duration of time the particles were pinning the contact line. In the later stages, both the particle chain and the drop edge were observed to move inward, but we also observed that very few new particles were arriving at the drop edge just before the drop edge started to move inward. Thus, for these two cases, we cannot claim unambiguously that the particles do not pin the contact line. For the 3 μl drop both the particle chain and drop edge had started moving inward much earlier in the process and one could notice more particles arriving from the bulk even as the contact line was receding. We also note that the time for drop evaporation is significantly greater for the 5 μl drop than for the 3 μl drop. The time for evaporation in a depinning drop with shrinking radius is generally significantly smaller than that for the pinned drop. This suggests that the behavior of 5 μl drop displayed more characteristics of a pinned drop than a depinned drop. Other factors being constant, we expect Ψ to increase with the increase in the drop volume. Thus, larger drops should favor pinning. Interestingly, Ψ for the 1.5 μl volume drop in our experiments was greater than that for the 3 μl volume drop perhaps because the humidity was different in the two experiments. Based on these observations, we believe that we had a clear case of depinning for the 3 μl volume drop and close to a pinned behavior for 1.5 and 5 μl volume drops. Ψ values for the latter may therefore be regarded as close to the critical value for pinning/depinning transition. We therefore estimate that

$$C \approx 0.2. \tag{55}$$

This estimate will be consistent with our theoretical estimate if we take n_c equal to 5, a reasonable number for the chains initially formed. We hasten to stress, however, that more experimental work is needed to confirm the theory for the reasons given below.

C. Discussion

One of the difficulties in determining if a given suspension drop depins according to the physics described in the present study is that ideally one must ensure that there are enough particles in the suspension to form a ring all around the circumference of the drop. Since the particles tend to nearly touch each other due to strong attractive capillary forces, the number of particles required to form at least one ring of touching particles is approximately given by $N = \pi R/a$. Equation (51) gives us an estimate of the time required to form a single particle-wide ring,

$$t^*_{ring} \equiv \frac{t_{ring}U_0}{h_0(0)} = \frac{\pi}{3\phi}\left(\frac{a^3}{R^2 h_0}\right)^{1/2}. \tag{56}$$

The nondimensional time t^*_{ring} for the ring formation for our experimental conditions is given in Table I. This time must ideally be much less than $\frac{1}{4}$, the nondimensional time for complete drop evaporation [cf. Eq. (54)]. We see that this condition was not satisfied for our 3 μm diameter particles with $\phi = 2.5 \times 10^{-4}$. We therefore had to examine the videos for the three volume cases carefully to determine if the depinning happened toward the end of the experiment or much earlier. Since our video was only focused on one long chain it is possible that we observed both pinning and depinning behaviors even though t^*_{ring} is comparably $\frac{1}{4}$.

As we mentioned earlier, our experiments were also affected by sedimentation. The Stokes sedimentation velocity $U_s = (2a^2\Delta\rho g)/(9\mu)$ for 3 μm diameter particles is about 2×10^{-5} cm/s. In 3 min, the particle settles about 40 μm. This is about 10–15 % of the drop height. Thus, after about 3 min the volume fraction of the particles arriving near the drop edge could have been reduced by about 15% and therefore the actual value of C might be that much greater. For 10 μm diameter particles the sedimentation velocity is ten times greater and almost all the particles settle out. Thus even though the case of $\phi = 0.01$, $2a = 10$ μm, and $V = 5$ μl suspension listed in Table I gives $\Psi = 0.25$, we did not observe pinning. Finally, we should also mention that our theoretical estimate was based on small number of chains and the drag coefficient λ based on a single particle while we are really more interested in assessing if a ring formed could be stable enough to pin the contact line. We could have used the drag coefficient corresponding to long chain of particles, which, as mentioned earlier, could be O(40) or even higher. For very long chains, however, the effect of the particles on the contact angle also changes and it can shown that for the case of a ring all around the drop edge, one must replace $n_c\delta$ in Eq. (41) by $2R$. The resulting criterion for pinning, in lieu of Eq. (53), is $\phi \mathrm{Ca} R^4/(a^2 h_0^2) > 32/(9\lambda)$. For this criterion to compare well with the depinning observed for the 3 μm diameter particles, λ is required to be of O(200) or even greater. This appears excessively high drag coefficient even for a chain of particles but the limited data we have cannot be used to rule out this criterion.

Clearly, more carefully planned experiments are needed to establish the validity of the criteria derived here.

V. CONCLUSIONS

Deegan *et al.* [1,2] provided basic mechanism for the ring formation when a liquid containing particles is evaporated from a substrate. The main premise of that mechanism is that the evaporation rate near the drop edge is much greater than near the drop center. The presence of the particles near the contact line causes the contact line to remain pinned and causes the liquid from the bulk of the drop to move toward the drop edge causing thereby an accumulation of the particles near the drop edge. We found that not all particles, however, are effective in pinning the contact line. The volume fraction of the particles must be large enough in order that the rate at which the drop-substrate contact angle decreases due to evaporation is offset by the increase caused by the new protruding particles. We suggest that the particles will pin the contact line only when the criterion given by Eq. (53) with $C \approx 0.2$ is satisfied. According to this criterion, whether the particles will facilitate the pinning of the contact line depends not only on the particle size but also on particle volume fraction, drop radius, evaporation rate, and the wetting characteristics of the substrate. More experiments, however, are necessary to establish the validity of this criterion.

ACKNOWLEDGMENT

The authors are grateful to Professor Peter G. Simpkins for many helpful discussions related to the problem described here.

APPENDIX A: GREEN'S FUNCTION FOR *N* PARTICLES IN A CIRCULAR DOMAIN

The Green's function satisfying Eqs. (23)–(25) is expressed as a sum of three parts,

$$G = G_s + G_r + G_v, \tag{A1}$$

where G_s corresponds to the Green's function with the N singularities in an infinite domain, G_r is a regular solution of the Laplace equation that renders $G_s+G_r=0$ at $r=R$, and G_v is a regular solution of Poisson equation that renders the integral of G over the circular domain $r\leq R$ to vanish.

Using the method of finite Fourier transforms, it can be shown that the singular part G_s is given by

$$G_s = \begin{cases} N \ln r - \sum_{j=1}^{\infty} (1/j)(r_0/r)^{jN} \cos(jN\theta), & r > r_0 \\ N \ln r_0 - \sum_{j=1}^{\infty} (1/j)(r/r_0)^{jN} \cos(jN\theta), & r < r_0. \end{cases} \tag{A2}$$

The regular part is given by

$$G_r = -N \ln R + \sum_{j=1}^{\infty} (1/j)(rr_0/R^2)^{jN} \cos(jN\theta) \tag{A3}$$

and the part concerned with the volume of the liquid is given by

$$G_v = N\left(1 - \frac{r^2}{R^2}\right)\left(1 - \frac{r_0^2}{R^2}\right). \tag{A4}$$

For the purpose of determining h near a particle at $r=r_0$ and $\theta=0$, we need an expansion of G around that point,

$$G = \ln|\vec{r} - \vec{r}_0| - (N\sigma^2/R^2)(1 - r_0^2/R^2) + \sum_{m=0}^{\infty} g_m \sigma^m \cos m\varphi, \tag{A5}$$

where $\sigma=|\vec{r}-\vec{r}_0|$. Note that the first term on the right-hand side of the above equation corresponds to the Green's function for an isolated singularity at $\vec{r}_0$ in an infinite domain for which an equivalent Fourier series expansion is given by

$$\ln|\vec{r} - \vec{r}_0| = \begin{cases} \ln r - \sum_{j=1}^{\infty} (1/j)(r_0/r)^{j} \cos(j\theta), & r > r_0 \\ \ln r_0 - \sum_{j=1}^{\infty} (1/j)(r/r_0)^{j} \cos(j\theta), & r < r_0. \end{cases} \tag{A6}$$

To determine the constants g_m in Eq. (A5), we combine Eqs. (A5) and (A6) to yield, along $\theta=0$ and for $r>r_0$,

$$\begin{aligned} G^r &\equiv G - \ln|\vec{r} - \vec{r}_0| \\ &= (N-1)\ln r - N \ln R \\ &\quad + \sum_{j=1}^{\infty} (1/j)[(r_0 r/R^2)^{jN} - (r_0/r)^{jN} + (r_0/r)^{j}] + G_v. \end{aligned} \tag{A7}$$

Now using the Taylor series expansion

$$\ln(1-y) = -\sum_{j=1}^{\infty} (1/j) y^j, \tag{A8}$$

we obtain

$$G^r = \ln\left[\frac{1}{r}\left(\frac{r}{R}\right)^N \frac{1-(r_0/r)^N}{1-(r_0/r)} \frac{1}{1-(rr_0/R^2)^N}\right] + G_v. \tag{A9}$$

The constants g_m in Eq. (A5) can now be evaluated from the values G_r and its derivatives at $r=r_0$. Thus, for example, $g_0=G^r(r=r_0)$. Using L'Hopital's rule we obtain

$$g_0 = \ln\left[\frac{N r_0^{N-1}}{R^N} \frac{1}{1-(r_0/R)^{2N}}\right] + N\left(1 - \frac{r_0^2}{R^2}\right)^2. \tag{A10}$$

Similarly, the coefficient g_1 is obtained by evaluating the radial derivative of G_r at $r=r_0$, which yields Eq. (31) given in the main text.

APPENDIX B: CAPILLARY FORCE ON A PARTICLE (MODEL A)

The force along the gas-liquid-particle contact line is given by (Paunov *et al.* [16])

$$\vec{F}_\gamma = \oint \gamma[\cos\theta_p \vec{dl} \times \vec{n}_p + \sin\theta_p \vec{n}_p dl], \tag{B1}$$

with integration being along the contact line. In the above equation, $\vec{dl}$ represents the tangent vector along the contact line. The first term on the right-hand side of the above equation is the component of the force tangent to the surface of the sphere, while the second one is along the normal to the surface of the particle. In the cylindrical coordinate system passing through the test particle placed along the x_1 axis, we have

$$\vec{dl} = \left[\frac{dh_c}{d\varphi}\vec{e}_z + \frac{d\sigma_c}{d\varphi}\vec{e}_\sigma + \sigma_c \vec{e}_\varphi\right] d\varphi, \tag{B2}$$

where $[h_c(\varphi), \sigma_c(\varphi)]$ represent the liquid height and the contact line radius along the contact line as functions of θ. Since the particles are equispaced, the net force on the test particle is along the x_1 axis. Using Eq. (15) for $\vec{n}_p$, we find that

$$\begin{aligned} \oint (\vec{dl} \times \vec{n}_p)_1 = \frac{1}{a}\int_0^{2\pi} d\varphi[&\cos\varphi \sigma_c (h_c - a) \\ &- \sin\varphi\{\sigma_c dh_c/d\sigma_c - (h_c - a)\} d\sigma_c/d\varphi], \end{aligned} \tag{B3}$$

where the subscript 1 refers to the x_1 component of the inte-

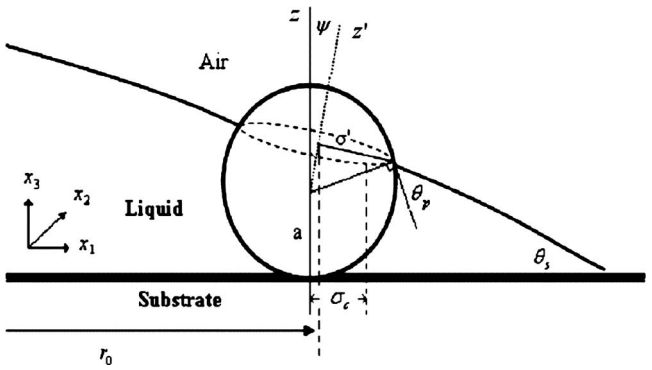

FIG. 6. An alternate model for the contact line.

grand. Substituting for σ_c from Eqs. (19) and (32) and using boundary conditions (20) and (21) along the contact line, one obtains

$$\oint (\vec{dl} \times \vec{n}_p)_1 = -2\pi\sigma_1 \sin\theta_0 \tan\theta_0. \tag{B4}$$

Next, we have

$$\oint (\vec{n}_p dl)_1 = \int_0^{2\pi} (\sigma_c/a)\cos d\varphi \times [\sigma_c^2 + (dh_c/d\varphi)^2 + (d\sigma_c/d\varphi)^2]^{1/2} \cong \int_0^{2\pi} (\sigma_c^2/a)\cos\varphi d\varphi = 2\pi\sigma_1 \sin\theta_0.$$

Here, the terms involving squares of $\sigma_c^{-1} dh_c/d\varphi$ and $\sigma_c^{-1} d\sigma_c/d\varphi$ are neglected with a relative error of $O(\theta_s^2)$.

Combining the two integrals we obtain

$$F_{\gamma,1} = -2\pi\gamma\sigma_1 \tan\theta_0 \sin(\theta_0 - \theta_p). \tag{B5}$$

The force due to uneven pressure distribution is given by

$$\vec{F}_p = -4\gamma s \int \vec{n}_p dA, \tag{B6}$$

where the integration is to be carried out over the liquid-wetted surface of the particles. It can be shown that the component of this force along the x_1 axis is given by

$$F_{p,1} = -\pi\gamma s\sigma_1 a[-\sin\theta_0 \tan\theta_0 + \cos\theta_0 - \cos\theta_p]. \tag{B7}$$

APPENDIX C: ALTERNATE MODEL FOR CONTACT LINE (METHOD B)

An alternate model of the contact line at particle surface is depicted in Fig. 6. Here, we assume that the contact line is a circle in a plane inclined at an angle ψ to the normal to the substrate. Let σ' be the radius of the contact line and φ' be the polar angle in a cylindrical coordinate system with its z' axis aligned along the normal to the contact line plane. The formal solution is still given by Eq. (22) with r_0 being now defined as the distance of center of the contact line from the centerline of the drop. As before, we truncate Eq. (22) to keep only the terms with A_0 and A_1. Next, we multiply boundary conditions (16) and (17) by $d\varphi'$ and $\cos\varphi' d\varphi'$ and integrate from $\varphi'=0$ to $\varphi'=2\pi$, generating thereby a total of four equations in the unknowns, A_0, A_1, r_0, and ψ for selected values of σ_0, θ_p, θ_s, and a/R. The equations were nonlinear and were solved using an iterative method. Knowing r_0, ψ, and σ_0, the position of the center of the particle, and hence h_∞, the height of the liquid in the absence of the particle, can be determined. The capillary force on the particle can be determined using Eq. (B1). Simpson's rule was used in all numerical integrations involved in satisfying boundary conditions (16) and (17) in the integral sense as described above and for determining the capillary force.

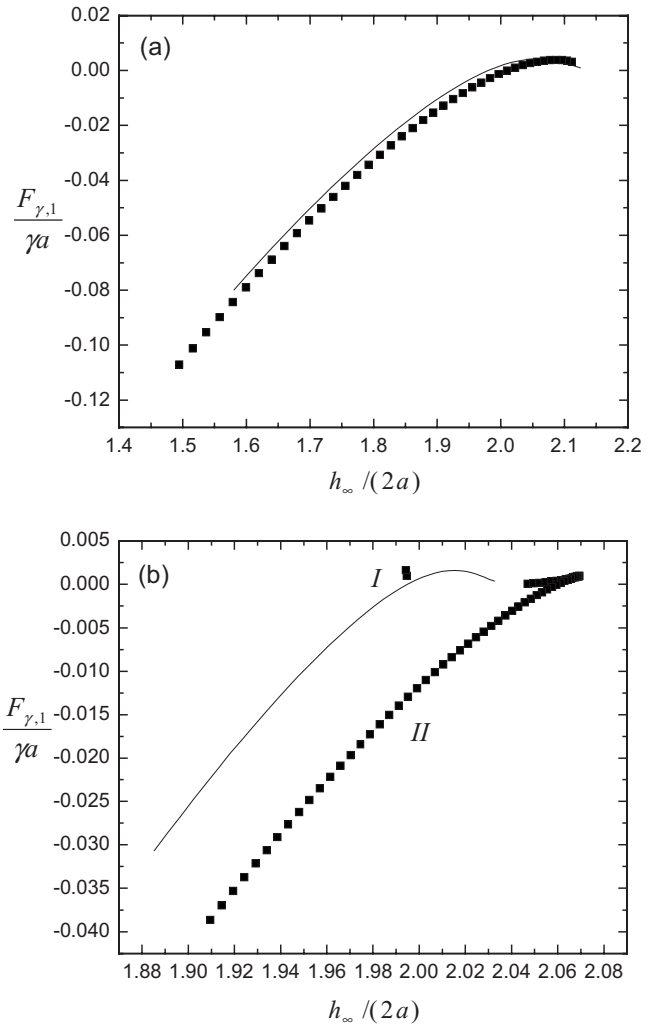

FIG. 7. A comparison of the two models. The solid line represents the first model and the squares represent the alternate model. (a) θ_p=0.2, θ_s=0.1; (b) θ_p=0.1, θ_s=0.15. For both cases, N=1, R=2 mm, and a=0.5 μm. I and II denote the two branches of the solution predicted by method B.

Figure 7 compares the results obtained by the two models. When θ_s is small compared to θ_p, the contact line plane is nearly parallel to the substrate, and the predictions from the two models are in good agreement [cf. Fig. 7(a)]. Figures 7(b) and 8 show the results for $\theta_p < \theta_s$, for which case model

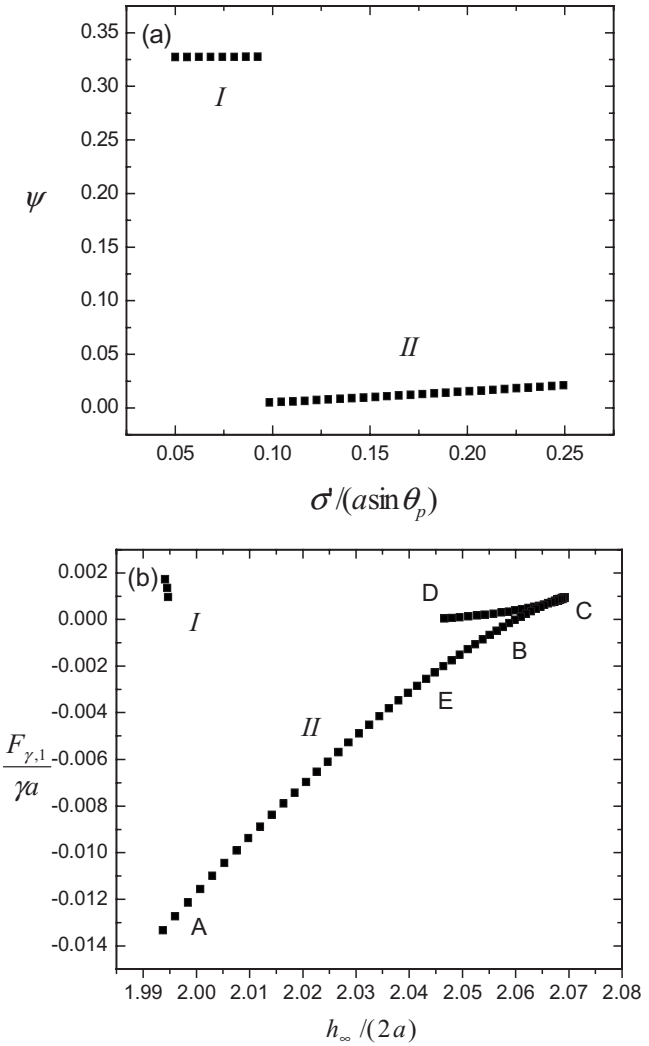

FIG. 8. Details of branch I and II solutions. (a) The contact line plane inclination as a function of the contact line radius. (b) The capillary force as a function of h_∞.

A predicts $\sigma_1 > \sigma_0$ for some radial positions of the particle. According to model B, two solutions are possible for some radial positions of the particles. As seen in Fig. 8, there is an abrupt transition from a branch of solutions in which the contact line plane is significantly inclined to the substrate to the one in which the contact line is approximately parallel to the substrate. The former branch, referred to as branch I, occurs only for small values of the contact line radius σ', as can be seen in Fig. 8(a), which shows the angle ψ as a function of σ'. In branch I, the angle ψ is approximately given by

$$\psi = \theta_s + \cos^{-1}(\cos\ \theta_s \cos\ \theta_p). \tag{C1}$$

As shown in Fig. 8(b), the capillary force is positive for branch I, indicating that the capillary force will push the particle outward toward the drop edge resulting in the increase in protrusion and hence σ' beyond the critical value (approximately equal to $0.07a \sin\ \theta_p$ for the case shown in Fig. 8) for which there is an abrupt transition to branch II. Thus, the branch I solution is unlikely to be observed in practice. Note that branch I occurs over very small range of radial position and force and therefore appears essentially as a point in Figs. 7(b) and 8(b). [σ' variations in Figs. 7(b) and 8(b) are much greater than in Fig. 7(a).] A transition from branch I to branch II, in which the contact line plane is approximately parallel to the substrate, will lead to a state indicated by D in the Fig. 8(b). Since the capillary force at D is positive, the particle will be forced outward toward the drop edge. However, the particle cannot move toward the drop edge as there is no continuation of the solution in branch II beyond D. Note, however, that there are two solutions for h_∞ corresponding to D (denoted by D and E). σ' for E is much greater than for D. The capillary force for state E is negative and the particle will move radially inward, along EB. At B, the force is zero and the particle will reach the equilibrium position (provided that we completely neglect the viscous force).

Alternatively, we may examine what happens to a particle that is carried by the fluid and first protrudes from the gas-liquid interface, i.e., at $h_\infty = 2a$, represented by A in Fig. 8(b). The capillary force at A is negative and therefore the particle will move inward along AEB and will come to rest at B where the capillary force is vanishingly small. The next particle carried by the fluid will first protrude at a point indicated by C for which h_∞ is the highest and r_0 is the smallest. The capillary force there is positive and the particle will move outward along CE until it comes to rest at E. In summary, regardless of what the conditions are when the particle protrudes, it will quickly come to the only equilibrium state denoted by E. Note that the force versus particle position curve is nearly independent of N, so that all particles would roughly stop at essentially the same radial position. This is consistent with the observation made earlier (cf. Fig. 1).

[1] R. D. Deegan, O. Bakajin, T. F. Dupont, G. Huber, S. R. Nagel, and T. A. Witten, Nature (London) **389**, 827 (1997).
[2] R. D. Deegan, O. Bakajin, T. F. Dupont, G. Huber, S. R. Nagel, and T. A. Witten, Phys. Rev. E **62**, 756 (2000).
[3] Y. O. Popov, Phys. Rev. E **71**, 036313 (2005).
[4] V. N. Truskett and K. J. Stebe, Langmuir **19**, 8271 (2003).
[5] N. D. Denkov, O. D. Velev, P. A. Kralchevsky, I. B. Ivanov, H. Yoshimura, and K. Nagayamat, Langmuir **8**, 3183 (1992).
[6] N. D. Denkov, O. D. Velev, P. A. Kralchevsky, I. B. Ivanov, H. Yoshimura, and K. Nagayamat, Nature (London) **361**, 26 (1993).
[7] C. D. Dushkin, K. Nagayama, T. Miwa, and P. A. Kralchevsky, Langmuir **9**, 3695 (1993).
[8] E. Adachi, A. S. Dimitrov, and K. Nagayama, Langmuir **11**, 1057 (1995).
[9] C. Gigault, K. Dalnoki-Veress, and J. R. Dutcher, J. Colloid Interface Sci. **243**, 143 (2001).
[10] J. Jing, J. Reed, J. Huang, X. Hu, V. Clarke, J. Edington, D.

Housman, T. S. Anantharaman, E. J. Huff, B. Mishra, B. Porter, A. Shenker, E. Wolfson, C. Hirot, R. Kantor, C. Aston, and D. C. Schwartz, Proc. Natl. Acad. Sci. U.S.A. **95**, 8046 (1998).
[11] L. Shmuylovich, A. Q. Shen, and H. A. Stone, Langmuir **18**, 3441 (2002).
[12] K. Su, M.S. thesis, Syracuse University, New York, 2005.
[13] C. Liu, M.S. thesis, Syracuse University, New York, 2006.
[14] S. M. Troian, E. Herbolzheimer, and S. A. Safran, Phys. Rev. Lett. **65**, 333 (1990).
[15] A. S. Sangani and C. Yao, Phys. Fluids **31**, 2426 (1988).
[16] V. N. Paunov, P. A. Kralchevsky, N. D. Denkov, I. B. Ivanov, and K. Nagayama, Colloids Surf. **67**, 119 (1992).
[17] S. S. Ozarkar and A. S. Sangani, Phys. Fluids **20**, 063301 (2008).
[18] J. R. Smart and D. T. Leighton, Phys. Fluids A **1**, 52 (1989).
[19] J. R. Smart, S. Beimfohr, and D. T. Leighton, Phys. Fluids A **5**, 13 (1993).
[20] S. S. Ozarkar (private communication).
[21] A. S. Sangani and S. Behl, Phys. Fluids A **1**, 21 (1989).